Mon. Not. R. Astron. Soc. **303,** 1–14 (1999)

Photoelectric heating for dust grains at high redshifts

Biman B. Nath,[1⋆] Shiv K. Sethi[2⋆] and Yuri Shchekinov[3,4⋆]

[1]*Raman Research Institute, Bangalore 560080, India*
[2]*Institut d'Astrophysique, 98 bis, Boulevard Arago, 75014 Paris, France*
[3]*Osservatorio Astrofisico di Arcetri, Largo E. Fermi 5, 50125 Firenze, Italy*
[4]*Department of Physics, Rostov State University, Sorge 5, 344090, Rostov on Don, Russia*

Accepted 1998 September 22. Received 1998 September 7; in original form 1997 July 31

ABSTRACT

Lyman-α absorption systems at $z \sim 3$ with $N_{\rm HI} \gtrsim 3 \times 10^{14}$ cm^{-2} have been found to be enriched with a mean metallicity of $Z/Z_\odot \sim 10^{-2.5}$, and a large scatter in the metallicity. It is reasonable to assume that the process of initial enrichment of the intergalactic medium (IGM) at $z \gtrsim 3$ also produced dust grains. We explore the implications of the presence of dust grains in the IGM at high redshift, in particular, the contribution of photoelectric emission from grains by hard background photons to the net heating rate of the IGM.

We show that (i) the charge on dust particles and the characteristics of photoemitted electrons differ substantially from those in the interstellar medium (ISM) in several respects: (a) grains are exposed to and charged by photons beyond the Lyman limit, and (b) because of this, the photoelectrons have typical energy of tens of eV. We also show that: (ii) silicates are more efficient heating agents than graphites; (iii) small grains contribute mostly to the net heating; (iv) at densities typical of the IGM at $z \sim 3$ and for Lyα absorbers, dust heating can be comparable to or exceed photoionization heating within an order of magnitude; and (v) this increases the temperature of overdense regions, compared to the case of no dust heating, by a factor of $\sim$2. We discuss the implications of this extra heating source in Lyα absorbing systems.

Key words: methods: analytical – dust extinction – intergalactic medium – quasars: absorption lines – early Universe.

1 INTRODUCTION

Recent observations with high resolution have provided evidence for the existence of heavy elements in Lyman-α (Lyα) forest clouds at redshifts $z \sim 3$ (Cowie et al. 1995; Tytler et al. 1995). Songaila & Cowie (1996) claimed that more than 75 per cent of all Lyα absorbers with $N_{\rm HI} \gtrsim 10^{14}$ cm^{-2} at $z \sim 3$ are enriched. Tytler et al. (1995) reported similar results: all Lyα systems with $N_{\rm HI} \gtrsim 10^{15}$ cm^{-2} and 60 per cent with $N_{\rm HI} \gtrsim 10^{14}$ cm^{-2}. These values are expected to be lower limits, since the measurements of heavy elements are limited by signal-to-noise ratio, and all Lyα systems may contain heavy elements (see also Tytler 1988).

The abundance of metals, however, remains somewhat uncertain, especially because it depends on the value of the ionization parameter (Γ, the ratio of ionizing photon density to the particle density) assumed. Nevertheless, for a reasonable range of $\Gamma = 10^{-1.5}$–$10^{-2.5}$, the inferred metallicity is almost independent of the H I column density, and is of order $Z/Z_\odot \sim 10^{-2}$ (Songaila & Cowie 1996). Rauch, Haehnelt & Steinmetz (1997) found from the comparison of the data with their numerical simulations that the metallicity has a mean $\sim 10^{-2.5}$ solar and that there is a large scatter. Songaila (1997) has recently reported a lower limit to the metallicity of order $\Omega_{\rm metals}/\Omega_{\rm b} \sim 1\text{-}4 \times 10^{-5}\, h\,(1 + 2q_{\rm o}z)^{1/2}$. For a low-$q_{\rm o}$ Universe ($q_{\rm o} = 0.02$), $h = 0.65$ and a solar metallicity of 0.019, this implies a minimum metallicity of order $10^{-3.3}$–$10^{-2.8}$ solar.

Recent studies of metallicity and dust content in nearby galaxies have demonstrated that dust-to-gas ratio k and metallicity $\zeta = Z/Z_\odot$ are correlated (Schmidt & Boller 1993; Lisenfeld & Ferrara 1998). Though the correlation is not always good, it definitely shows that the production of metals in galaxies is accompanied by dust formation. Moreover, weak correlation between k and ζ in blue compact dwarf galaxies may indicate that galaxies during active phases of star formation eject dust along with metals in gaseous outflows (Lisenfeld & Ferrara 1998). It is, therefore, reasonable to expect that if the intergalactic medium (IGM) and Lyα absorbers are enriched with metals, they are also contaminated with dust grains, produced inside the galaxies and transported into the IGM along with metals. The presence of dust in the IGM and its consequences was first discussed by Rowan-Robinson, Negroponte & Silk (1979), who suggested that dust in the early Universe at $z \sim 200$ could lead to distortions of cosmic microwave background

⋆E-mail: biman@rri.ernet.in (BBN); sethi@iap.fr (SKS); yus@rsuss1.rnd.runnet.ru (YS)

radiation (CMBR) (see also Vainer 1990; Loeb & Haiman 1997). More recently, Fall, Pei & McMahon (1989) and Pei, Fall & Bechtold (1991) have argued that the reddening of background quasars indicates directly that dust grains exist in damped Lyα systems. Their dust-to-gas ratio ranges from $k = 0.06$ to $k = 0.35$ for different extinction curves assumed (here $k = 10^{21}\tau_{\rm B}/N_{\rm H\,I}$, $k_{\rm G} = 0.79$ for the Galaxy; Fall & Pei 1989). Arguments based on the extinction of light by dust have led Zuo et al. (1997) to similar estimates of k in damped Lyα clouds towards the lensed quasar 0957+561. They explain the difference in the continuum shape of the two spectra by differential reddening as a result of the presence of dust grains. Recently, however, Pettini et al. (1997) have shown that the dust-to-metals ratio in damped Lyα systems is only $\simeq$1/2 of its value in local interstellar clouds (thus, dust-to-gas ratio is $k \simeq k_{\rm G}\zeta/2$). They infer this from the fact that Cr and other refractory elements are depleted only by a factor of 2 in 18 studied damped Lyα systems, much less than in the interstellar medium (ISM), and assuming that this depletion is caused by freezing on dust grains.

In this paper we assume that dust particles are present not only in damped Lyα systems, but also in Lyα forest clouds, following the idea that dust is associated with metals. We concentrate here on detailed study of dust charging in the high-redshift IGM illuminated by the background ultraviolet (UV) and X-ray photons and heating by injected suprathermal photoelectrons – in several respects these processes differ from those in the local interstellar medium.

We do not discuss here how metals and dust particles are supplied to the IGM; we refer the reader to papers where the IGM enrichment has been associated with Population III stars (Ciardi & Ferrara 1997; Gnedin & Ostriker 1997), early-forming very massive objects (Carr, Bond & Arnett 1984) and galactic winds from galaxies at high redshifts (Silk, Wyse & Shields 1987; Miralda-Escudé & Rees 1997; Nath & Trentham 1997). The estimates show that an enriched IGM with a metallicity of $10^{-2.5}$ Z$_\odot$ at $z \sim 3$ can be understood in terms of either Population III objects or galactic winds.

The paper is structured as follows. In Section 2 we describe the basic processes and the equations, in Section 3 we describe the basic characteristics of charged high-redshift dust particles exposed to the background UV radiation and photoemitted electrons, and in Section 4 we present the results of the evolution of temperature in the IGM with photoinduced dust heating as an important energy source. We then briefly discuss the implication of our results for Lyα absorbers. Throughout the paper we use a Hubble constant $H_0 = h_{50}\,50$ km s^{-1} Mpc^{-1} and $\Omega = 1$.

2 THE CHARGE OF A DUST GRAIN IN THE IGM

2.1 The UV background radiation

We first discuss the ambient photon background, which is important for the process of charging of the dust at high redshift. The existence of a UV background radiation at high redshift has been inferred from proximity effect observations (Bajtlik, Duncan & Ostriker 1988). These observations show that the UV background radiation has an intensity at $\lambda = 912$ Å of $J_{912,-21} \sim 0.3$–1, in units of 10^{-21} erg s^{-1} cm^{-2} sr^{-1} Hz^{-1} ($2 < z < 3$) (Bechtold 1994; Cristiani et al. 1995; Cooke, Espey & Carswell 1996).

On the theoretical front, following the pioneering work of Miralda-Escudé & Ostriker (1990), several authors have calculated the expected value of $J_{912,-21}$ from quasars, using existing quasar luminosity functions, and taking into account the absorption of photons by the intervening Lyα absorption systems (e.g. Madau 1992; Haardt and Madau 1996). This predicted intensity, however, falls short of the inferred intensity from the proximity effect (Cooke et al. 1996). It has, therefore, been suggested that there are other sources of UV photons at high redshift, e.g. young star-forming galaxies, decaying neutrinos, or even a warm, collisionally ionized IGM. The predicted *spectrum* of the UV background in these cases however is much different, and, therefore, observational constraints on the spectrum hold the clue to the origin of the high-redshift UV background radiation. The observations of He II absorption at high redshift put constraints on the spectrum of the ionizing background (Jakobsen et al. 1994; Davidsen, Kriss & Zheng 1996). Meiksin & Madau (1994) showed that the He II opacity observed by Jakobsen et al. (1994) suggests that the softness ratio, $S_{\rm L} \equiv J_{912}/J_{228} \gtrsim 40$ at $z \sim 3.3$ assuming a reasonable value of the opacity caused by diffuse H I (see also Songaila, Hu & Cowie 1995). For the Davidsen et al. (1996) observations, Sethi & Nath (1997) found that the allowed range of models is still large, after taking various uncertainties into account ($16 \lesssim S_{\rm L} \lesssim 650$). There have been recent claims that the spectral index changes around $z \sim 3$ (Songaila 1998; Reimers et al. 1997; Hogan, Anderson & Rugers 1997; Savaglio et al. 1997), but we assume a constant spectral index for simplicity. We discuss the effect of such a change in Section 3.3.

Table 1. Models for the UV background radiation.

λ(Å)	QSO	QSO+YG
$\lambda = 912$(Å)	$J_{-21} = 0.5$	$J_{-21} = 1.0$
$228 < \lambda$(Å)$ < 912$	$J_\nu \propto \nu^{-0.5}$	$J_\nu \propto \nu^{-2.5}$
$\lambda = 228$(Å)	$J_{-21} = 0.025$	$J_{-21} = 0.00123$
$\lambda < 228$(Å)	$J_\nu \propto \nu^{-1}$	$J_\nu \propto \nu^{-1}$
$S_{\rm L}(\equiv J_{912}/J_{228})$	20	813

For our purpose here, we will use two models for the UV background radiation for our calculation, bearing in mind the above uncertainties. The first one (referred to as QSO) represents the background radiation expected from only quasars or quasi-stellar objects, and the second one (QSO+YG) represents the radiation expected from quasars or quasi-stellar objects and young galaxies. The models are described in Table 1. The model QSO is a broken power-law fit to the spectrum obtained by Haardt & Madau (1996), for an intermediate redshift of $z \sim 2.5$. Note that their calculation was actually for $q_{\rm o} = 0.1$. The model QSO+YG assumes the QSO luminosity function of Boyle (1991), as in Madau (1992), and a population of young galaxies, which is used to make $J_{912,-21} = 1$ using the A3 model of absorption of Giroux & Shapiro (1996) (again at $z \sim 2.5$; see also Sethi & Nath 1997). The values of the softness ratio $S_{\rm L}$ for each model are given in Table 1. Although broken power laws are crude approximations to the actual spectrum, they suffice for our purpose of illustrating the effect of dust charging and heating at high redshift, in the light of the uncertainty in our knowledge of the UV background radiation.

Beyond 228 Å, we use $J_\nu \propto \nu^{-1}$ till $h\nu = 3$ keV for both models. This again mimics well the Haardt & Madau (1996) spectra for $10\,\text{Å} \lesssim \lambda \lesssim 228\,\text{Å}$. For $E_\gamma \gtrsim 3$ keV, we use the quasar X-ray spectral index of 0.9. Zdziarski et al. (1995) found a good fit to the data for Seyfert galaxies with a spectral index of 0.9 till ~100 keV. However, photons with energies much above 1 keV do not contribute significantly in the charging and heating processes because of the small absorption coefficients at these energies.

The evolution of the background radiation in redshift also remains uncertain. For simplicity, we assume that $J_{912,-21}$ remains constant for $2 < z < 5$, and $J_{912,-21} \propto (1+z)^{2.8}$ for $z < 2$. This is a fit

to the evolution of $J_{912,-21}$ as calculated by Madau (1992) for $z < 2$. Also, we assume that the spectral shape remains constant in time, although in reality the spectrum becomes softer at higher redshift as a result of an increase in absorption (Miralda-Escudé & & Ostriker 1990). Again, however, the uncertainties involved are large, and we assume a constant spectral shape for simplicity.

2.2 Basic processes for charging grains

In this paper we follow Draine (1978) and Draine & Salpeter (1979, hereafter DS) in describing the processes determining the grain charge. The equation governing the charge on a grain is written as follows:

$$\frac{\mathrm{d}q}{\mathrm{d}t} = 4\pi a^2 e \Sigma_{\mathrm{i}} J_{\mathrm{i}} \,, \tag{1}$$

where J_{i} is the partial current due to particles of the i th kind, and a is the grain radius. The currents that mainly determine grain charge in the ISM are caused by: (i) impinging electrons, (ii) impinging ions (mainly protons) and (iii) UV photons. In principle, secondary processes can be associated with these three (such as secondary electron emission); however, under the conditions in which we are interested they play a minor role. In the case of incident electrons and protons, currents J_{i} are enhanced by Coulomb interaction by a factor $g(x)$. For electrons, with $x = eU/kT$, where U is the grain potential (Spitzer, 1978),

$$g_{\mathrm{e}}(x) = \begin{cases} \exp(x) & \text{if } x < 0, \\ 1 + x & \text{if } x > 0. \end{cases} \tag{2}$$

For ions, it is given by

$$g_{\mathrm{i}}(x) = \begin{cases} \exp(-zx) & \text{if } x > 0, \\ 1 - zx & \text{if } x < 0, \end{cases} \tag{3}$$

where z is the ion charge.

2.2.1 The current resulting from impinging electrons

Grain particles in low-density IGM exposed by UV and X-ray photons are positively charged, and the electron current can be written as (DS)

$$J_{\mathrm{e}} = -n_{\mathrm{e}} \left(\frac{kT}{2\pi m_{\mathrm{e}}}\right)^{1/2} (\langle s_{\mathrm{e}} \rangle - \langle \delta \rangle)(1 + x) \,, \tag{4}$$

where $\langle s_{\mathrm{e}} \rangle$ is the thermally averaged sticking probability for incident electrons. This probability $\langle s_{\mathrm{e}} \rangle \simeq 1$ for thermal electrons with temperature T and grain size a satisfying the condition (Draine, 1989)

$$a > 10 \left(\frac{T}{10^6 \mathrm{K}}\right)^{1.5} \text{Å} \,, \tag{5}$$

which is valid for temperature $T \leq 10^5$ K, the range of temperatures relevant in our case. $\langle \delta \rangle$ is the secondary emission coefficient; for incident thermal electrons with $kT \ll 300$–500 eV, $\langle \delta \rangle \ll 1$.

2.2.2 The current resulting from impinging ions (protons)

DS give, for the proton current,

$$J_{\mathrm{ip}} = n_{\mathrm{p}} \left(\frac{kT}{2\pi M}\right)^{1/2} (z\langle s_{\mathrm{p}} \rangle + \langle \nu_{\mathrm{p}} \rangle - \beta \langle Y_{\mathrm{p}} \rangle) \exp(-x) \,, \tag{6}$$

where $\langle s_{\mathrm{p}} \rangle \simeq 1$ is the effective sticking coefficient, $\langle \nu_{\mathrm{p}} \rangle \ll 1$ is the secondary electron emission coefficient, and $\beta \langle Y_z \rangle \ll 1$ is the charging arising from sputtered charge particles, as can be estimated from DS for temperature $T \leq 10^5$ K. It is seen clearly that, in fully ionized IGM, the contribution of protons to grain charging is of order $|J_{\mathrm{p}}| \sim 0.03|J_{\mathrm{e}}|$. We neglect the current from helium ions, since for the situations with which we are concerned in this paper, the contribution from ions is in general small compared to electron and photoinduced currents.

2.2.3 Photoelectric current per area

Photoelectric current per grain area is

$$J_{\mathrm{UV}} = \int_{\nu_{\min}}^{\infty} Q(a, \nu) y_\nu \frac{4\pi J_\nu}{h\nu} \, \mathrm{d}\nu \,, \tag{7}$$

where J_ν is the spectral energy flux of incident photons (erg cm^{-2} s^{-1} Hz^{-1} sr^{-1}), y_ν the photo-yield, i.e. the number of photoemitted electrons per absorbed photon, $Q_\nu(a)$ the efficiency of photoabsorptions, and $\nu_{\min} = (w + eU)/h$ corresponds to the minimum energy for which electrons can escape from the surface of a dust grain, w being the workfunction. The normalized photo-yield can be written as (Draine 1978; Bakes & Tielens 1994, hereafter BT)

$$y_\nu = y_0 \left(1 - \frac{I_z}{h\nu}\right) f_z(a) \,, \tag{8}$$

where (Draine 1978)

$$f_z(a) = \left(\frac{\zeta}{\alpha}\right)^2 \frac{(\alpha^2 - 2\alpha + 2 - 2e^{-\alpha})}{(\zeta^2 - 2\zeta + 2 - 2e^{-\zeta})} \,, \tag{9}$$

with

$$\alpha = \frac{a}{l_{\mathrm{a}}} + \frac{a}{l_{\mathrm{e}}}, \qquad \zeta = \frac{a}{l_{\mathrm{a}}} \,, \tag{10}$$

where a is the grain radius, l_{a} the photon attenuation length, and l_{e} the electron escape length; BT give $l_{\mathrm{a}} = 10^{-6}$ cm and $l_{\mathrm{e}} = 10^{-7}$ cm. The asymptotic (at photon energies much larger than the ionization potential of a grain I_z) value of y_0 is determined by Draine (1978) as $y_0 = 0.5$ to reproduce the enhanced value of the photo-yield of a small particle over bulk graphite, and by BT as $y_0 = 0.14$ to fit experimental data for coronene (Verstraete et al. 1990). I_z is the ionization potential for a grain with charge Z (BT), and is given by

$$I_z = w + (Z + \frac{1}{2}) \frac{e^2}{a} \,. \tag{11}$$

Here e is in esu units. It is important to note here that when the photoinduced current is calculated for the ISM in the Galaxy, the upper limit in the integral is defined as the Lyman limit frequency ν_{L} (Drain 1978; BT), regarding the fact that Lyman continuum photons are confined within H II regions. This places an upper limit on the charge of dust grains, the energy of photoemitted electrons and thus the photoelectric heating. In our case, charging of dust grains and photoelectric heating are determined by photons with energy above the Lyman limit. BT stress that near threshold the photo-yield for graphite grains is usually overestimated. In our case, with photon energies and electric potentials much higher than in the ISM, the contribution from the threshold region is small.

2.2.4 Photoabsorption efficiency

For silicate particles Q can be reasonably approximated for sizes $a \leq 0.1\mu$m with which we are concerned and photon energies $\epsilon \geq 10$ eV by (Ferrara & Dettmar 1994)

$$Q(a, \epsilon) = \left(\frac{\epsilon}{8\mathrm{eV}}\right)^{\gamma_{\mathrm{a}}} \,, \tag{12}$$

where

$$\gamma_a = 2.5\left[(10a)^{0.1} - 1\right]. \quad (13)$$

Here and throughout the paper a is in μm, if not specified.

For graphite particles, we use the approximation

$$\begin{aligned} Q(a,\epsilon) =& 30 \times a \exp(-11.9\sqrt{a})\sigma_1(\epsilon) \\ &+ 60 \times \frac{a}{1+25a}\exp(-7.5\sqrt{a})\sigma_2(\epsilon) \\ &+ \frac{10a}{(1+a)(1+10a)}\sigma_3(\epsilon), \end{aligned} \quad (14)$$

where σ_i, the cross-sections per carbon atom in a particle (in megabarns), are described below. For σ_1 and σ_2, we used the data given in BT (see their fig. 1), which we approximated as

$$\sigma_1(\epsilon) = \begin{cases} 5.24\times10^{-4}\epsilon^{3.78}, & \epsilon \le 17.29\,\mathrm{eV}, \\ 1.37\times10^{5}\epsilon^{-3.02}, & \epsilon > 17.29\,\mathrm{eV}, \end{cases} \quad (15)$$

$$\sigma_2(\epsilon) = \begin{cases} 0.032\epsilon^{2.5}, & \epsilon < 6.13\,\mathrm{eV}, \\ 112.7\epsilon^{-2}, & \epsilon > 6.13\,\mathrm{eV}, \end{cases} \quad (16)$$

$$\sigma_3(\epsilon) = 1.5 + 2\times10^{-4}(\epsilon - 0.22)(\epsilon - 18)(\epsilon - 40)\,, \quad (17)$$

where ϵ is given in eV. This approximation for $Q(a,\epsilon)$ agrees with the results of Draine & Lee (1984) (see their fig. 4) for grain sizes $a = 0.03$–0.1 and with the results of BT (see their fig. 1), which are based on an extrapolation of the results of Draine & Lee to smaller particles, to within 10–15 per cent for $3\,\mathrm{eV} \lesssim \epsilon \lesssim 40\,\mathrm{eV}$, and 20–30 per cent for $\epsilon \lesssim 3\,\mathrm{eV}$. BT showed that the ionization cross-sections obtained in this way are in good agreement with the data for the small polycyclic aromatic hydrocarbon coronene (Verstraete et al. 1990).

At energies $\epsilon > 40\,\mathrm{eV}$, for $Q(a,\epsilon)$, we use the approximation given by DS,

$$Q(a,\epsilon) = Q(a, 40\,\mathrm{eV})\left(\frac{40\,\mathrm{eV}}{\epsilon}\right); \quad (18)$$

and for $\epsilon > 1$ keV,

$$Q(a,\epsilon) = Q(a, 1\,\mathrm{keV})\left(\frac{1\,\mathrm{keV}}{\epsilon}\right)^3. \quad (19)$$

These approximations give reasonable fits (within 10–15 per cent) in the entire energy range. One should stress however that, in the high-energy interval $\epsilon \gtrsim 1$ keV, the $Q(a,\epsilon) \propto \epsilon^{-3}$ dependence is contaminated by very sharp increases in Q when the photon energy approaches the edge of an atomic subshell, and can exceed the $Q(a,\epsilon) \propto \epsilon^{-3}$ value by 1–1.5 orders of magnitude (Dwek & Smith 1996). From this point of view our results for dust charging and heating can be considered conservative.

2.3 Grain potential

It is readily seen from the charge equation that characteristic charging times caused by the photoinduced and electron currents, for $n_e \ge 10^{-7}$ cm^{-3}, are much shorter than the Hubble time at $z \lesssim 20$ ($t_H \sim 10^{15}$ s) and sound crossing time for a cloud with $R > 1$ kpc with temperature $T \sim 10^4$–10^5 K ($t_R \sim 10^{15}$ s). Therefore, the grain charge is kept at equilibrium, $\dot{q} = 0$, and can be easily determined from

$$n_e\left(\frac{8kT}{\pi m_e}\right)^{1/2}(1+x) = \int_{\nu_{\min}}^{\infty} Q(a,\nu)y_\nu \frac{4\pi J_\nu}{h\nu}\,\mathrm{d}\nu + n_p\left(\frac{8kT}{\pi m_p}\right)^{1/2}. \quad (20)$$

It is clear that the proton current can be comparable to the photoinduced current when the particle flux for protons $\sim n_p v_p$ is comparable with the photon flux $\sim J_\nu/h$. More precisely, for a power-law spectrum $J_\nu \propto \nu^{-\alpha}$ this is equivalent to the condition

$$\left(\frac{8kT}{\pi m_p}\right)^{1/2} n_p \sim \frac{4\pi Q y J_0}{\alpha h}\left(\frac{h\nu_L}{w}\right)^{\alpha}, \quad (21)$$

where J_0 is the spectral energy flux at the Lyman limit frequency ν_L, and Q and y are the absorption efficiency and photo-yield averaged over the spectrum. For typical values $J_0 \sim 10^{-21}$, $Q \sim 0.1$ and $y \sim 0.1$, this is equivalent to $n_e \sim 0.2T_4^{-1/2}$. Thus, for conditions in the IGM at $z \sim 3$ photoinduced current dominates dust charging.

2.3.1 Analytical estimates

For grains exposed to hard UV radiation, the charge and potential are expected to be high, $x \gg 1$, and can be estimated for a power-law spectrum of incident photons $J \propto \nu^{-\alpha}$ and a power-law dependence for $Q(a,\nu) \propto Q(a,\nu_L)(\nu/\nu_L)^{-\beta}$, as

$$x \sim \left[\frac{10^{\alpha+\beta-2}}{n_e T_4^{\alpha+\beta+1/2}(\alpha+\beta)}Q(a,\nu_L)\right]^{1/(\alpha+\beta+1)}. \quad (22)$$

Here, we have used $y = 0.1$; our assumption of $x \gg 1$ is valid for $n_e < 10^{-3}$–10^{-4} cm^{-3}, and $T_4 < 10$. For $\alpha \sim 1$, $\beta \sim 3$ (such β is typical for graphite particles of small sizes in the energy interval $\epsilon = 17.3$–40 eV), this gives a weak dependence of the potential on gas density and absorption characteristics,

$$x \sim 2n_e^{-0.2}T_4^{-0.9}[J_{-21}Q(a,\nu_L)]^{0.2}.$$

In Lyα clouds with $n_e \sim 10^{-4}$ cm^{-3} and $T \sim 10^4$ K ,

$$x \sim 10[J_{-21}Q(a,\nu_L)]^{0.2},$$

which is much larger than the value for grains in the local ISM illuminated by photons below the Lyman limit. For graphite particles with larger radius, $a \sim 0.1$, $\beta \sim 1$–1.5, and

$$\begin{aligned} x \sim\ & 0.8n_e^{-0.25}T_4^{-0.6}[J_{-21}Q(a,\nu_L)]^{0.25} \\ & - n_e^{-0.28}T_4^{-0.86}[J_{-21}Q(a,\nu_L)]^{0.28}. \end{aligned}$$

Silicate particles have less strong dependence of $Q(a,\epsilon)$ on photon energy in the interval $\epsilon > 10$ eV, $\beta \sim 0$–1 for $a = 0.1$–0.001, respectively, which results in a stronger dependence of grain potential on the parameters of the ambient medium:

$$\begin{aligned} x \sim\ & 0.3n_e^{-0.5}T_4^{-0.75}[J_{-21}Q(a,\nu_L)]^{0.5} \\ & - 0.8n_e^{-0.33}T_4^{-0.83}[J_{-21}Q(a,\nu_L)]^{0.33}. \end{aligned}$$

Note that the dependence of the graphite grain potential on $Q(a)$ and on grain size is weaker than for silicates.

2.3.2 Numerical results

Figs 1(a) and (b) show the dependence of grain potential $x = eU/kT$ for graphites and silicates, respectively, on the ambient density for hard (QSO) and soft (QSO+YG) spectra of background photons, for a grain size of $a = 10^{-5}$ cm and for fixed gas temperature $T = 10^4$ K. Figs 2(a) and (b) show the dependence of x for graphites and silicates on the grain size a for different ambient densities for the QSO and QSO+YG spectra.

The figures show that the dependences follow qualitatively the above simple estimates. In general, the hard spectrum (QSO) results in higher value of x, especially for silicates, and both graphites and

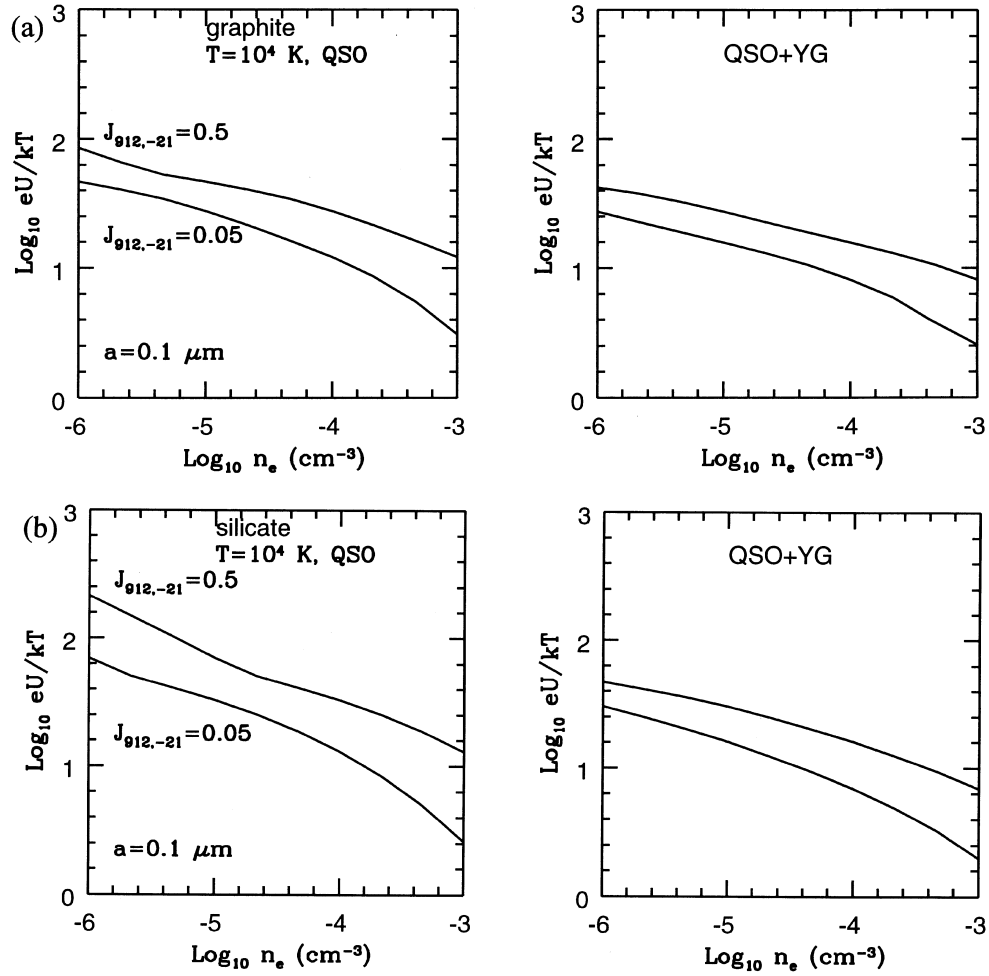

Figure 1. (a) Grain potential eU/kT plotted against ambient density $n_{\rm e}$ for QSO and QSO+YG spectra for graphites for two values of $J_{912,-21} = 0.5$ and 0.05 and for $a = 10^{-5}$ cm. (b) Same as (a) but for silicates.

silicates have comparatively lower grain potentials for the soft spectrum. QSO spectra with low equivalent α result in a stronger dependence of grain potential on density than do QSO+YG spectra with larger equivalent α. Graphites do not show much dependence of the potential on the grain size, while silicates do, which is the result of the weaker dependence of $Q(a,\epsilon)$ on photon energy for silicates, as seen from analytical estimates. It is also seen that grain potential on silicate particles depends on the ambient density more strongly than on graphite particles.

2.4 Photoelectric heating

The heating rate as a result of the photoelectric effect in dust grains (in erg cm^{-3} s^{-1}) is given by

$$H_{\rm ph} = n_{\rm H} \int {\rm d}a\, \mathcal{N}_{\rm g}(a)\sigma(a) \times \int_{\nu_{m1(a)}}^{\infty} {\rm d}\nu\, Q(a,\nu) y_\nu \frac{4\pi J_\nu}{h\nu} [h\nu - w - eU(a)]\,, \quad (23)$$

where $\nu_{m1(a)} = (w + eU + 3kT/2)/h$ is the minimum frequency of photons needed to eject electrons that have sufficient energy to heat the surrounding gas, and $\mathcal{N}_{\rm g}(a) = {\rm d}n/{\rm d}a$, the size distribution of grains, is taken to be a power law $\mathcal{N}_{\rm g}(a) = Aa^{-q}$. The normalizing factor A can be determined from

$$A \int_{a_{\rm min}}^{a_{\rm max}} a^{-q} \frac{4}{3}\pi\rho_{\rm g} a^3\, {\rm d}a = 10^{-2}\zeta m_{\rm H} n\,, \quad (24)$$

where $a_{\rm min} = 5\times10^{-7}$ cm and $a_{\rm max} = 4\times10^{-5}$ cm (see O'Donnel & Mathis 1997) are the minimal and maximal sizes of dust particles, respectively. Then, the coefficient A is

$$A = 3.8\times10^{-27}(4-q)\left(\frac{Z}{Z_\odot}\right)\frac{n}{a_{\rm max}^{4-q} - a_{\rm min}^{4-q}}\,, \quad (25)$$

for typical grain density $\rho_{\rm g} = 1$ g cm^{-3}. For $U(a)$ in equation (23), we use the results for grain charge as obtained in Section 2.3.

2.4.1 Mean energy of photoelectrons

An important parameter that determines the photoelectric heating is the mean energy of photoemitted electrons,

$$E(a) = \frac{\int_{\nu_{\rm min}}^{\infty} {\rm d}\nu\, Q(a,\nu) y_\nu \frac{4\pi J_\nu}{h\nu}[h\nu - w - eU(a)]}{\int_{\nu_{\rm min}}^{\infty} {\rm d}\nu\, Q(a,\nu) y_\nu \frac{4\pi J_\nu}{h\nu}}\,. \quad (26)$$

In the local interstellar medium $E(a)$ is of the order of

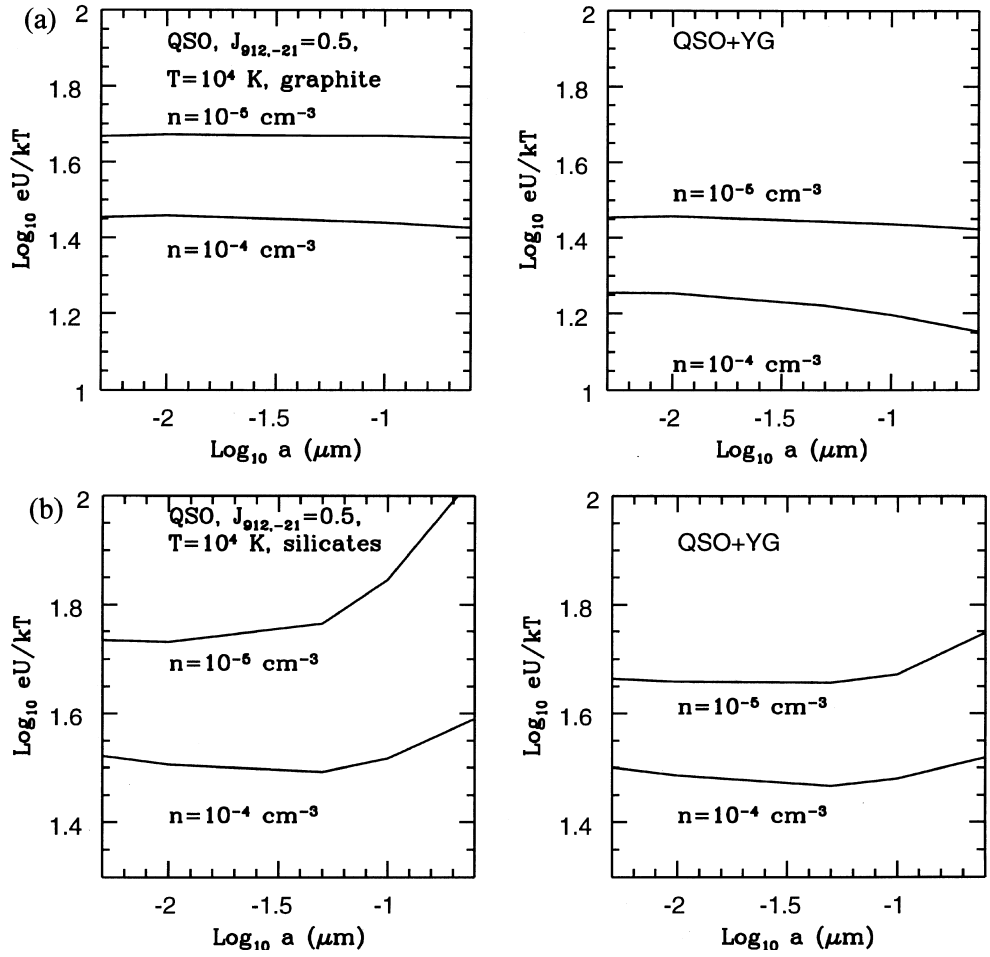

Figure 2. (a) Grain potential plotted against a for graphites for two incident photon spectra (QSO and QSO+YG) for $J_{912,-21} = 0.5$ and 0.05, and for $n_e = 10^{-5}$ and 10^{-4} cm^{-3}. Same as in (a) but for silicates.

$h\nu_L - w \sim 5.6$ eV. In a medium exposed to hard UV photons it is restricted only from below, and the exact value depends on the UV spectrum. Figs 3 and 4 show this dependence for graphite and silicate particles. It is seen that $E(a)$ can reach hundreds of eV at low densities, while typical values for moderate densities are 30–50 $kT\sim$ tens of eV.

Note that, although the curves in Figs 3 and 4 show that in general $E(a)$ for grains with higher charges is large, it should not be taken to mean that higher charge *causes* the mean electron energies to be larger. The dependence of $E(a)$ on eU/kT at $T = 10^4$ K is shown in Fig. 5 for silicates (solid lines) and graphites (dotted lines), for QSO type (thick lines) and QSO+YG type spectra (thin lines) (the upper set of curves are for $a = 10^{-5}$ cm and the lower set of curves are for $a = 10^{-6}$ cm). It is seen that $E(a)$ is a monotonically increasing function of eU/kT, and the nature of the curve depends on $Q(a, \nu)$, y_ν and the photon spectrum.

The differential heating rate (per unit grain) is a product of absorbed photons and $E(a)$,

$$\frac{dH_{ph}}{dn_g(a)} = E(a) \int_{\nu_{m1(a)}}^{\infty} d\nu\, Q(a,\nu) y_\nu \sigma(a) \frac{4\pi J_\nu}{h\nu},$$

and can be therefore roughly estimated as

$$dH_{ph}(a)/dn_g(a) \propto E(a)(eU)^{\beta+\alpha-1} \propto E(a) n_e^{(\beta+\alpha-1)/(\beta+\alpha+1)},$$

i.e. flatter than linear.

2.4.2 *Differential heating rates*

Using the approximate solution for dust potential that we found in section 2.3.1 we can estimate partial contributions to the total heating rate from silicates and graphites. In the integral

$$\frac{dH_{ph}}{dn_g(a)} = \int_{\nu_{m1(a)}}^{\infty} d\nu\, Q(a,\nu) y_\nu \sigma(a) \frac{4\pi J_\nu}{h\nu} [h\nu - w - eU(a)], \quad (27)$$

we can neglect w in comparison with $h\nu$ and eU, and using as above power laws for the flux J and absorption coefficient $Q(a, \nu)$ we get

$$\frac{dH_{ph}}{dn_g(a)} \simeq 4 \times 10^{-5} f(\alpha,\beta) \sigma(a) n_e^{\frac{\alpha+\beta-1}{\alpha+\beta+1}} \times T_4^{-\frac{\alpha+\beta-1}{2(\alpha+\beta+1)}} [J_{-21} Q(a, \nu_L)]^{\frac{2}{\alpha+\beta+1}}, \quad (28)$$

where $f(\alpha, \beta) \sim 1$. It is seen from this equation that the differential heating rate, for both graphite and silicate particles, depends rather weakly on grain radius through $Q(a, \nu_L)$, and thus the contribution from grains of small radius dominates because of the factor $\mathcal{N}_g(a) \propto a^{-q}$. However, the integrated heating rate is insensitive to the grain size distribution: for $Q^{2/\alpha+\beta+1} \sim a^\eta$, with $0 < \eta < 1$, the dependence of heating rate on q is close to being cancelled by the normalizing factor A in equation (25).

In Fig. 6 we show heating rates (per unit volume) arising from graphite and silicate particles, respectively, integrated over size distributions both for incident photon spectra, and for different size

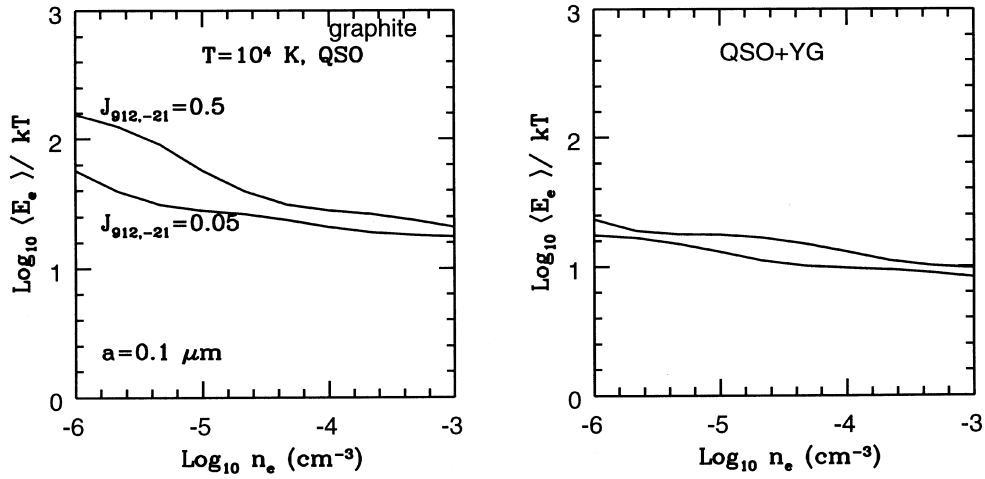

Figure 3. Mean energy of photoemitted electrons plotted against ambient density for $a = 10^{-5}$ cm, for QSO and QSO+YG spectra, for graphites.

distribution of grains, $q = 3.5$ and $q = 3.9$. For comparison we show also the photoionization heating rate for a primordial gas. It is seen that photoelectric dust heating depends on density less strongly than photoionization heating. Silicates produce a weaker dependence of heating rate on density, which can be explained by the weak dependence of grain potential and the mean energy of photoelectrons on density (see Figs 2 and 3). Owing to the fact that both eU and $E(a)$ for silicates are higher than for graphites, the heating rate by silicate grains is also higher. Changing the size distribution results in a weak change (within a factor of 1.5) of the heating rate: dust with $q = 3.9$ heats more efficiently than that with $q = 3.5$, as expected. In Fig. 7, we show the heating rate as a function of the lower limit of the grain size assumed, for different grain types and ambient densities. The curves show that the heating is dominated by small grains in general. In brief, in all cases the photoelectric dust heating is comparable to or even exceeds (at low densities) the photoionization heating.

The dependence of the dust heating rate on the ionizing radiation flux at the Lyman edge $J(\nu_{\rm L})$ is quite weak, particularly for QSO+YG spectra with large α. However, it can lead to variations in temperature as a result of local inhomogeneity in the exposing UV flux. On the other hand, the photoionization heating does not depend on the flux in a fully ionized medium with $n_{\rm HI} \ll n_{\rm H}$ for low density ($n \ll 10^{-3.5}$ cm^{-3} as considered here), as the photoionization heating rate is proportional to the recombination rate and thus weakly depends on the UV flux.

Under appropriate conditions dust heating can also stimulate spatial variations in temperature via thermal instability. In the simplest case of steady energy balance, $\Lambda(T)n^2 = H_{\rm ph}$, with $H_{\rm ph}$ depending on density and temperature as given in equation (28), Field's criterion for thermal instability of condensation mode (Field 1965) is written as

$$\frac{{\rm d}\log\Lambda}{{\rm d}\log T} - 1 + \frac{3}{2}\frac{\alpha+\beta-1}{\alpha+\beta+1} < 0, \qquad (29)$$

which shows that for $\alpha + \beta < 1$ (hard spectrum and dominance of silicate grains with $a > 0.01\mu$m), dust heating works as a destabilizing factor.

3 THERMAL EVOLUTION OF THE CLUMPY IGM WITH DUST HEATING

Next, we compute the thermal evolution of the clumps in the IGM with overdensities of order $\sim$10, which either keep their overdensity constant (i.e. adiabatically expand), or are confined by some mechanism and keep their density constant. These are described below in detail as Models I and II.

We assume that the gas in Lyα systems evolves passively, driven

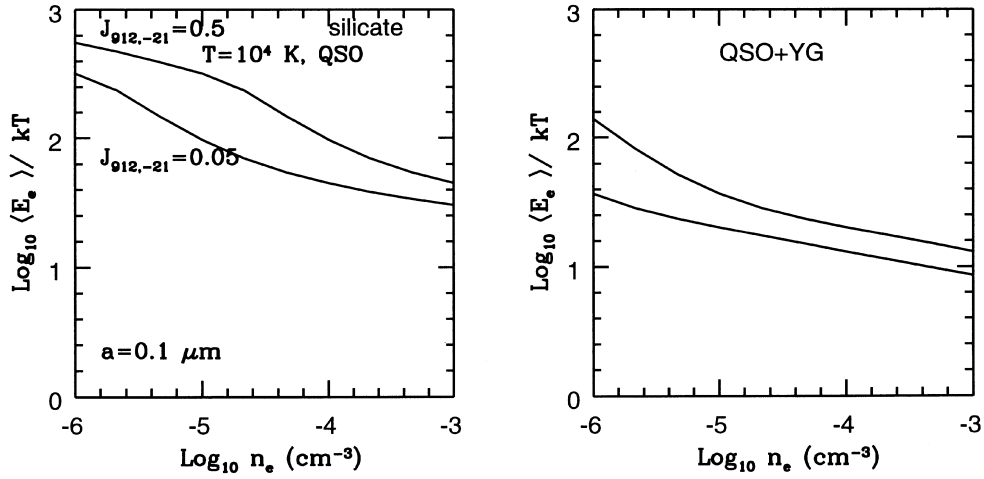

Figure 4. Same as in Fig. 3 but for silicates.

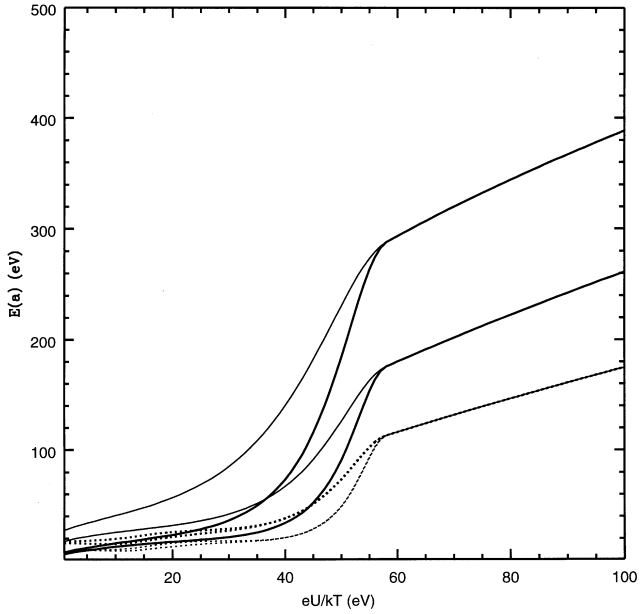

Figure 5. The mean electron energy $E(a)$ plotted against eU/kT for various sizes, photon spectra and grain types, at $T = 10^4$ K. The solid lines are for silicates and the dotted lines are for graphites. The thicker lines refer to QSO and thinner lines denote QSO+YG type spectra. The upper set of curves are for $a = 10^{-5}$ cm and the lower set for $a = 10^{-6}$ cm.

by the UV background flux and the expansion (or non-expansion) of the cloud. This is consistent with the picture of Lyα systems as described by the recent numerical simulations (e.g. Miralda-Escudé et al. 1996) in which Lyα system gas is not involved in star formation and is not affected by the processes related to it.

We note here that Miralda-Escudé & Rees (1994) also calculated the evolution of temperature in overdense regions of IGM, which first collapse under gravity, during which the temperature rises to $\sim 10^5$ K through adiabatic heating, and then evolve with constant (proper) density, during which, because of high density and the consequent high recombination and line cooling rate, temperature falls quickly to $\sim 10^4$ K. They, however, considered much higher densities ($\gtrsim 10^{-3}$ cm^{-3}) than we use here ($\lesssim 10^{-4}$ cm^{-3}) (at lower densities, the balance between the heating and cooling processes will be different, for example, adiabatic cooling will be more important).

The evolution of temperature in an overdense region in the IGM would depend on the initial temperature (and epoch) assumed. If the gas in the overdense region were initially compressed adiabatically, then the maximum temperature would be $T_{\rm cl} \sim (\rho_{\rm cl}/\rho_{\rm IGM})^{2/3}\, T_{\rm IGM}$, where $\rho_{\rm cl}$ is the density in the overdense region. For overdensities of order 5–10, that are considered to be typical values for Lyα absorbing systems (see below), $T_{\rm cl} \sim 3\text{-}5\, T_{\rm IGM}$. The value of $T_{\rm IGM}$, however, depends on the thermal history of the IGM (Miralda-Escudé & Rees 1994), which remains uncertain. Therefore, for the sake of illustrating the importance of dust heating, we

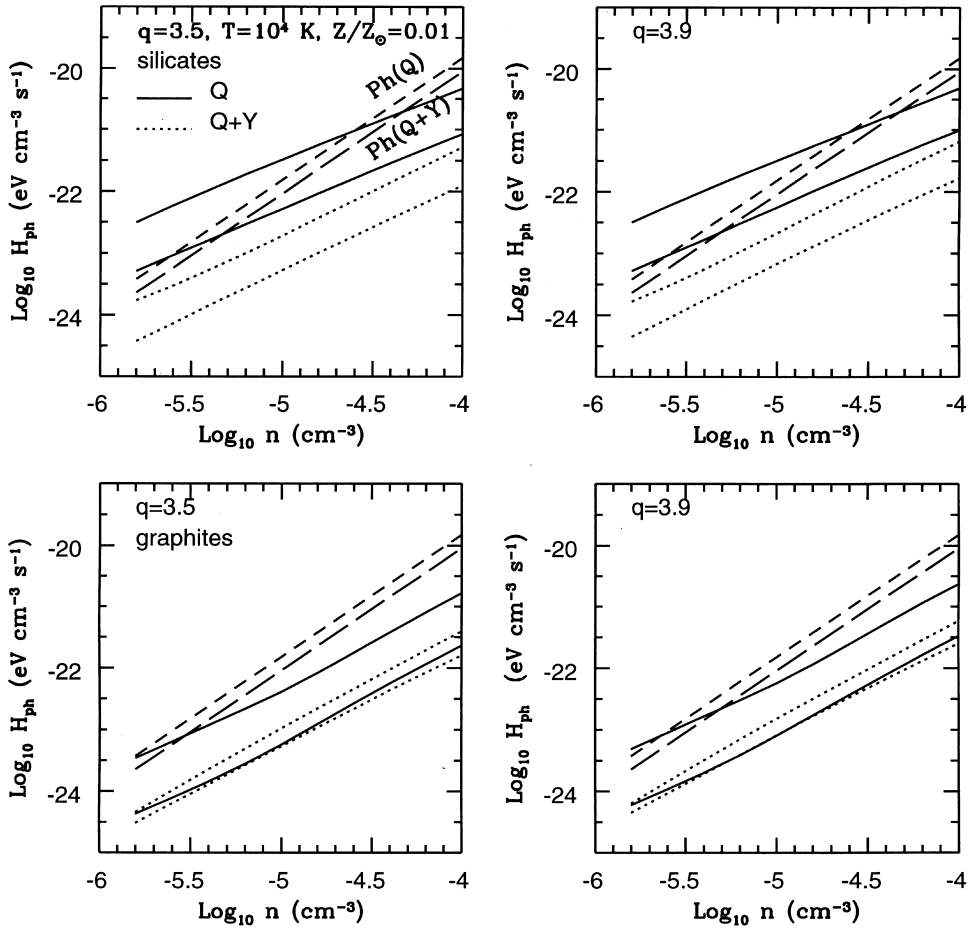

Figure 6. Integrated (over size distribution) heating rate for graphites and silicates versus ambient density for QSO (solid lines) and QSO+YG (dotted lines) spectra. The upper set of curves are for $J_{912,-21} = 0.5$ and the lower set for $J_{912,-21} = 0.05$. Photoionization heating rate for a primordial gas is shown for QSO (short dashed lines) and QSO+YG (long dashed lines).

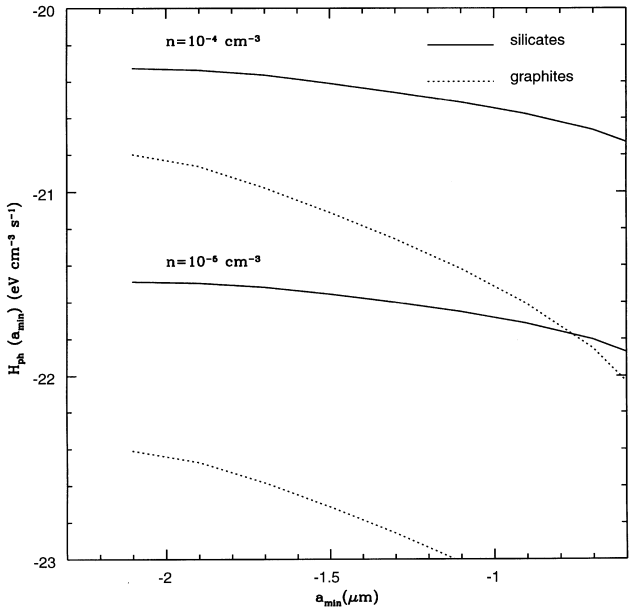

Figure 7. The heating rate as a function of the lower limit of the grain size (a), for silicates (solid lines) and graphites (dotted lines) for two different densities $n = 10^{-4}$ and 10^{-5} cm^{-3}, for QSO spectrum and at $T = 10^4$ K.

assume a few values of the initial temperatures of the overdense region $T_{\rm in}$ that are of order 10^4 K, and follow the thermal evolution in time.

3.1 Models: heating and cooling processes

In numerical calculations we used the heating rate caused by the photoelectric effect in dust grains as described above with grain size distribution $\mathcal{N}_{\rm g} \propto a^{-q}$ with $q = 3.5$. For the relative fraction of graphites and silicates, we use the one given by Pei (1992) for the Large Magellanic Cloud (LMC), which seems suitable for low-metallicity objects at high redshift (Pei et al. 1991). We also show the thermal evolutions with only graphites and silicates involved. The case of only silicates corresponds to the Small Magellanic Cloud (SMC) type dust grains (Pei 1992). For other heating processes apart from dust heating, we use photoionization heating of a primordial gas, for both models of UV radiation. The heating caused by photoionization of carbon atoms is smaller than this by a factor of 3 (10) for the QSO+YG (QSO) spectrum for a metallicity of $Z/Z_\odot = 0.01$. For cooling, we use recombination cooling, cooling through collisional ionization, line cooling (in the presence of UV radiation) and bremsstrahlung for a primordial gas, as given in Cen (1992). Cooling via heavy elements at this metallicity and temperature is unimportant. Inverse Compton cooling at $z \lesssim 5$ is not important and is neglected here [the corresponding cooling time-scale is $t_{\rm iC} \sim 9 \times 10^{12}(1+z)^{-4}$ yr (Tegmark, Silk & Evrard 1993)].

In Model I, we assume that the overdense regions adiabatically expand keeping the overdensity constant in time. In this case, therefore, we also include cooling through adiabatic expansion. In Model II, we consider regions with constant (proper) density, in which the gas is confined by gravity or shock ram pressure, or some other confinement mechanism. For Model I, we use $\rho_{\rm cl}/\Omega_{\rm b}\rho_{\rm c} = 10$, for all redshifts, where $\rho_{\rm cl}$ is the density inside the cloud, $\rho_{\rm c}$ is the critical density and $\Omega_{\rm b}$ is the global mean baryon density in units of $\rho_{\rm c}$. For Model II, we use $\rho_{\rm cl}/\Omega_{\rm b}\rho_{\rm c} = 10$ (at $z = z_{\rm in}$) for different values of the initial redshift $z_{\rm in}$. We use $\Omega_{\rm b} = 0.03$ and initial temperature $T_{\rm in} = 10^4, 2\times10^4, 5\times10^4$ K. Our choice of the parameters follows the result of Cen & Simcoe (1997) that Lyα absorbers with $N_{\rm HI} \sim 10^{14}$ cm^{-2} had $\rho_{\rm cl}/\rho_{\rm b} \sim 10$ at $z \sim 3$ for $\Omega_{\rm b} \sim 0.03$. The minimum width of Lyα lines at $z \sim 4$ has been recently found to be $b = 15$ km s^{-1} (Kim et al. 1997). If the minimum width (in the distribution of b values) is considered to be the result of gas temperature (see below for more discussion on this), this corresponds to a temperature of $\sim 10^4$ K and proves the presence of overdense regions with such temperatures at $z \sim 4$. Here we consider the temperature evolution of such regions in time.

In reality, the gas in Lyα systems is expected to behave in a way that lies between our two models. Numerical simulations show that the structures in the IGM corresponding to Lyα forest absorption lines are sheet-like structures (Miralda-Escudé et al. 1996). The gas is confined in one dimension and flows along the sheet towards hemispherical vortices. Therefore, the density is expected to fall slower than $(1+z)^3$. Also, since these structures are transient, lasting about a Hubble time, our calculations would be relevant only on time-scales shorter than this.

3.2 Models: numerical results

We show the evolution of the gas temperature in Figs 8(a) and (b) for graphites and silicates. The dotted and solid lines refer to the cases without dust, and with dust with $\zeta = Z/Z_\odot = 0.01$. The plots show the evolution for various initial temperatures, for the two models of background photons (upper panels for QSO and lower panels for QSO+YG spectra). The case of silicates, of course, corresponds to the grain mixture of the SMC type (Pei 1992). In Fig. 9 we show the case of grain mixture of the LMC type (Pei 1992) for the QSO spectrum for three values of initial temperatures and metallicities.

It is seen that the dominant contribution to the heating comes from silicate grains for both types of spectra. This is because, for silicates, the absorption efficiency does not decrease with increasing photon energy as sharply as it does for graphites, and therefore the high-energy photons contribute substantially in this case. In the case with hard background spectrum (QSO), the dust heating is more efficient for the same reasons – as a result of the contribution of high-energy photons, and the high mean energy of photoemitted electrons. In Model I without dust heating, adiabatic cooling decreases temperature sharply, so that at $z = 1$–2 it is below 10^4 K. Dust heating is able to support temperature at the level $T \gtrsim 10^4$ down to $z = 0$. In Model II with dust heating, temperature is a factor of 1.5–2 higher than without dust heating. At $z < 1$ both photoionization and photoelectric heating decrease because of a decrease of the UV flux.

Since dust heating manifests itself better (compared to other sources of heating) at lower densities, it is conceivable that the diffuse, low-density, 'intercloud' component of the IGM, if any, would have a much different thermal history with dust than with only photoionization heating. The density of such a component remains, however, uncertain. Recent numerical studies show that most of the baryons in the IGM are in the overdense regions, leaving about 5 per cent in the diffuse component (Zhang et al. 1998). Their results show a fragmented IGM at high redshift, and they claim that even the 'diffuse' medium is also possibly fragmented into scales smaller than the resolution of the simulation. For $\Omega_{\rm b} = 0.03$ and $h_{50} = 1$, this corresponds to a density $\simeq 4\times10^{-9}(1+z)^3$ cm^{-3} (using 5 per cent of the baryons in the diffuse component). Judging from the heating curves of Fig. 6, such a component would be hotter

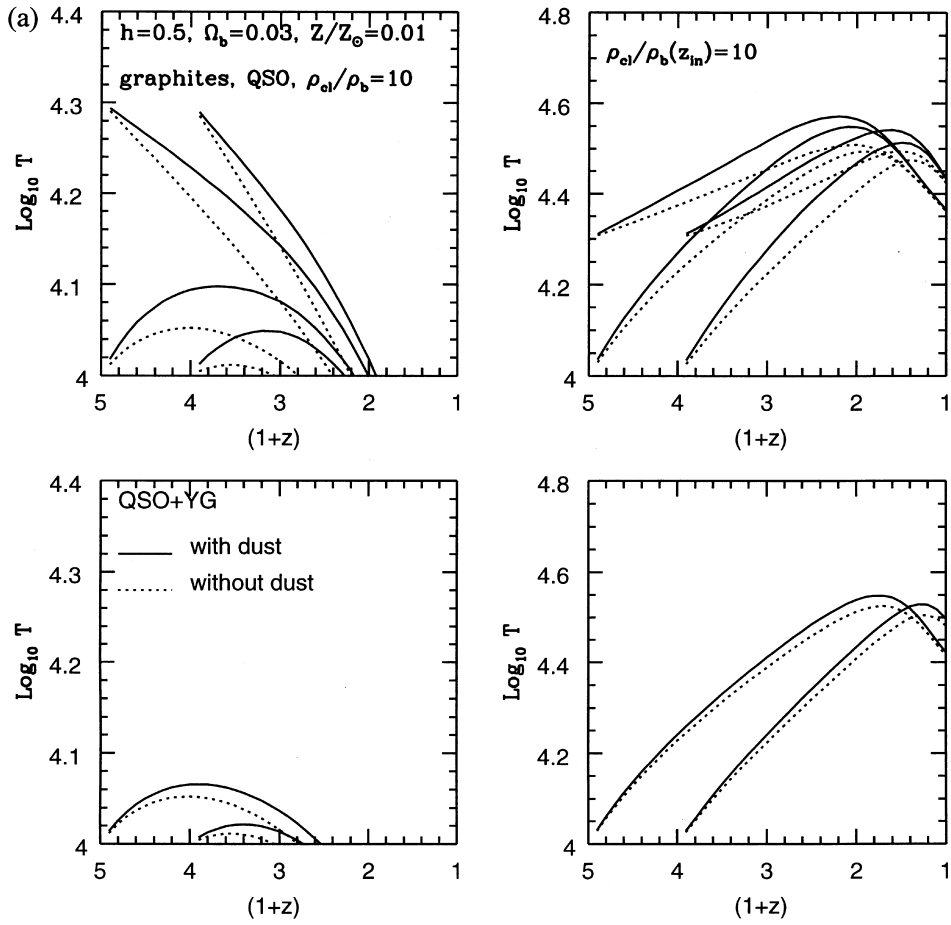

Figure 8. (a) Temperature evolution for clouds with constant density (left panels) and constant overdensity (right panels) for graphites. The evolution is shown for $z_{\rm in} = 3$ and 4. The top and bottom panels are for QSO and QSO+YG spectra respectively. The dotted lines show the case with only photoionization heating. The solid lines correspond to the case where dust heating is included for a metallicity of $Z/Z_{\odot} = 0.01$, for $\Omega_{\rm b} = 0.03$ and $T_{\rm in} = 10^4$ K. Thermal history with the QSO spectrum is added also with $T_{\rm in} = 2 \times 10^4$ K.

than if only photoionization is used. However, the temperature would depend on the thermal history of the IGM.

3.3 Uncertainties

Here we discuss briefly the effect of uncertainties in the parameters on our results. Since the type of dust particles in Lyα systems is uncertain, we showed the temperature evolution for different types of dust (graphite and silicate) in Figs 8(a) and (b). It is seen that the effect on the temperature of the gas is by factors of order $\lesssim$1.5. We also show the effect of different metallicities on the temperature evolution in Fig. 9, for $Z/Z_{\odot} = 0.003$ and 0.01. The difference in the temperature of the gas is again of order $\sim$1.5. Since the actual temperature evolution of the gas would depend on the initial conditions, readers are urged to use the heating rate shown in Fig. 6, and scale it for the required metallicity for different cases (the heating rate is proportional to the metallicity).

Finally, the evolution of the UV background radiation is still uncertain. For example, it has been claimed that the spectrum changes at $z \sim 3$ from soft at higher redshifts to a harder spectrum later (Songaila 1998 and references therein). We have already shown the heating rates (Fig. 6) and temperature evolution of the gas (Figs 8a and b) for a hard (QSO) and a soft (QSO+YG) spectrum, with the spectral index being constant in time. Figs 8(a) and (b) show that the temperature of the gas at later redshifts ($z \sim 2$) differs by very small factors for different values of $z_{\rm in}$. Since the heating rate for the soft spectrum case is very small compared to the hard spectrum case, a change in the spectrum at $z \sim 3$ would essentially be equivalent to the case of $z_{\rm in} \sim 3$, and, as explained above, it would affect the temperature evolution at later redshifts only negligibly. For $z_{\rm in} = 4$, the temperature would evolve much like the case of just photoionization between $3 \lesssim z \lesssim 4$ (dotted lines in Figs 8(a) and (b).

Similarly, the possibility that the value of $J_{912,-21}$ drops by a factor of 3-10 from $z \sim 2.5$ to $z \sim 4.2$ (Williger et al. 1994; Kim et al. 1997) would essentially mean a very small heating rate at $z \gtrsim 3$, but as explained above, it would not affect the temperature evolution at later redshifts much.

4 DISCUSSIONS

Finally, we discuss various implications of our results on photo-electric heating caused by dust in the IGM. To begin with, we discuss the plausibility of having dust in the IGM in the first place, i.e. the survival of dust grains in IGM.

4.1 Survival of dust particles

Before the discussion of the heating process attributable to dust,

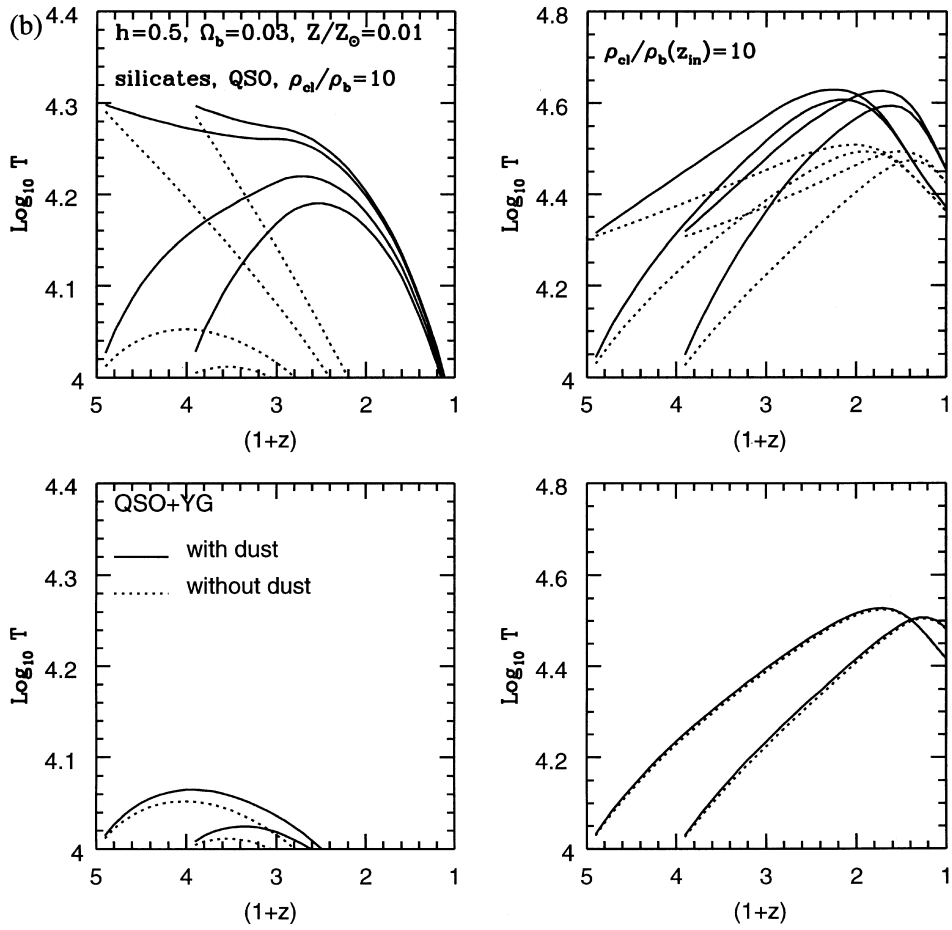

Figure 8. (b) The same as (a) but for silicates.

let us first consider the question of the survival of dust grains in high-redshift Lyman-α clouds. As already mentioned, these clouds have typical densities $\lesssim 10^{-4}\,\mathrm{cm}^{-3}$ at high redshift, have metallicities $\simeq 10^{-2.5}\,\mathrm{Z}_{\odot}$ and are exposed to background radiation $\simeq 10^{-21}$ erg cm^{-2} s^{-1} sr^{-1}. It is not clear if these clouds were enriched by metals driven out of earlier-generation dwarf galaxies with galactic winds or these metals come from in situ star formation; though the small scatter in observed metallicities as $N_{\rm HI}$ changes by over four orders seems to favour the former explanation (Cowie & Songaila 1998).

In the model of enriching the IGM by galactic winds at high redshifts (Silk et al. 1987; Miralda-Escudé & Rees 1997; Nath & Trentham 1997), the enriched gas is swept along with the ambient IGM by winds erupting out of dwarf galaxies as a result of the injection of energy by supernovae from an early bout of star formation. Dust grains could form either in the stars or in the shells of supernovae (Dwek 1998). Inside the parent galaxies, the processes of destruction of dust grains could be as efficient as in the Galactic ISM. The destruction of dust grains in our Galaxy is still not well understood (see McKee et al. 1987, and references therein). However, detailed modelling shows that it is reasonable to assume that a fraction ($\sim$10 per cent) of refractory dust survives the destruction process in ISM (Dwek 1998).

When the enriched material, presumably along with the dust grains, is ejected in the IGM, the destruction processes become less important. For sputtering, for example, the grain lifetime (above the sputtering threshold) is

$$t_{\rm sp} \sim \frac{N_{\rm a}}{Y_{\rm sp}}\frac{1}{\langle v\rangle n_{\rm s}\sigma_{\rm g}Q_{\rm coll}} \sim 6\times10^{13}\,\frac{1}{(Y_{\rm sp}/0.01)\,n_{\rm s}T_4^{1/2}}\ \mathrm{s}\,. \qquad (30)$$

Here, $N_{\rm a}$ is the number of heavy atoms in the grain, $Y_{\rm sp} \leq 0.01$ is the sputtering yield (number of atoms ejected from the grain per impinging atom) (Draine & Salpeter 1979), $\langle v\rangle$ is the thermal speed of the ambient particles with density $n_{\rm s}$ and temperature $T = T_4\,10^4$ K, $\sigma_{\rm g} = \pi a^2$ is the geometrical cross-section of the grains with radius a and $Q_{\rm coll}$ is a measure of the efficiency of collision. The numerical factor in the second expression assumes $N_{\rm a} = 3\times10^8$ and $a = 1\,\mu$m. In this equation, $n_{\rm s}$ is the density in the shell of the radiative shock ploughing through the IGM. Compare the above time-scale with the cooling time behind the shock (Shull & Silk 1981),

$$t_{\rm c} \sim 6\times10^{12}\,\frac{T_4^{1/2}}{(1+8.3\times10^3\,\zeta T_4^{-1/2})n_{\rm s}}\,\mathrm{s}\,, \qquad (31)$$

where $\zeta = Z/Z_{\odot}$. Therefore, dust can survive sputtering in the hot post-shock region before it cools.

The Lyman-α clouds are exposed to UV background radiation, which can potentially destroy the dust particles from sublimation. However, the intensity of background radiation is several orders below the ambient radiation in local H II regions and it can be shown that the grain temperature is close to that of the microwave background radiation (Loeb & Haiman 1997; Ferrara et al. 1998), which is too low for sublimation to be important.

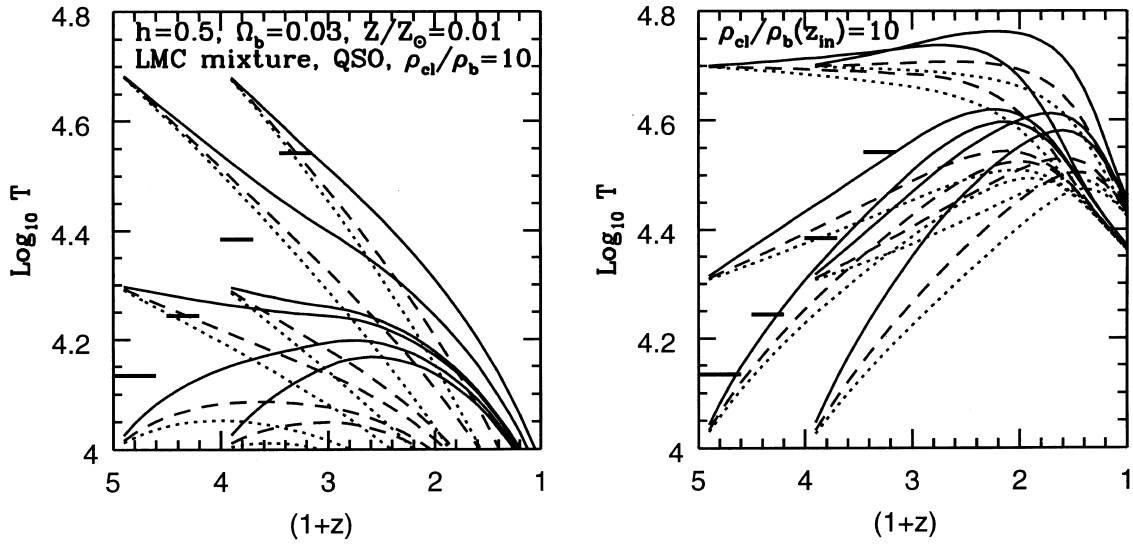

Figure 9. Temperature evolution for clouds with constant density (left panel) and constant overdensity (right panel) for QSO spectrum for a mixture of grains of LMC type. The evolution is shown for $z_{\rm in} = 3$ and 4. The dotted, dashed and solid lines correspond to the cases with only photoionization, and with dust with metallicities $Z/Z_\odot = 0.003$ and 0.01. The three sets of curves correspond to initial temperatures $T_{\rm in} = 1, 2, 5 \times 10^4$ K. The thick solid bars show the temperatures corresponding to the minimum b values from Kim et al. (1997).

If Lyman-α clouds are assumed to be star-forming regions then the UV flux inside these clouds can greatly exceed the background value (for dust heating we do not consider this case). From deep, serendipitous searches for redshifted Lyman-α and Hα emission lines, it is possible to put an upper limit on the ionizing intensity (or equivalently on the average star formation rate) inside the clouds (Hogan & Weymann 1987). These searches give upper limits which suggest that the hydrogen-ionizing flux inside the clouds does not exceed the background value by more than a factor of 10 (Thompson & Djorgovski 1995; Thompson, Mannucci & Beckwith 1996). As the dust grain temperature $T_{\rm d} \propto J_\nu^{1/5}$, this additional UV flux does not appreciably enhance it.

In the local ISM, other destruction mechanisms are cosmic ray erosion and shattering from dust collisions. The properties of cosmic rays at high redshifts are largely unknown. However, even if we assume the cosmic ray density in the clouds to be comparable to the local ISM, the time-scales of dust erosion are $\geq 10^{10}$ yr (Draine & Salpeter 1979). The time-scale of dust–dust collision in shocks in local ISM is $\simeq 10^8$ yr (Jones, Tielens & Hollenbach 1996). In Lyman-α clouds this time-scale would be larger by a factor of the square of the ratio of ISM to the cloud number density of grains. As this factor is $\geq 10^7$, dust–dust collision can be neglected as an important destruction mechanism. Also, since the magnetic field in the IGM is thought be small ($B \leq 10^{-9}$ G; Kronberg 1994), other destruction processes like non-thermal sputtering from betatron acceleration also become unimportant.

Therefore, we assume the dust-to-gas ratio to be proportional to that in Galactic ISM with a factor $\zeta = Z/Z_\odot$.

4.2 Lyα absorbers

It is clear from Figs 5, 6 and 7 that dust heating can play an important role in determining the physical state of the gas in Lyα absorbers, if they can be considered as overdense regions in the IGM. As mentioned in Section 3, the gas in Lyα absorbers is most likely to behave somewhere between the two extreme cases considered here, expand in two dimensions while being confined in one direction. In this case the gas would behave close to the evolution in Model I, and dust can heat up the gas instead of letting it cool.

The gas temperature in Lyα absorbers, however, is not directly observable. What is instead observed is the linewidth (the b value), and lines can be both thermally and velocity broadened. However, Haehnelt, Rauch & Steinmetz (1996) have argued that the minimum value of b in its distribution corresponds to the gas temperature, at least for lines with $N_{\rm HI} \gtrsim 10^{14}$ cm^{-2}. Numerical simulations seem to show that lines with lower column density are mostly velocity broadened (Miralda-Escudé & Rees 1997). In this context, it is interesting to note the recent observations of Kim et al. (1997). They used Keck spectra of five quasars at different redshifts and found that the minimum value of b increased in time. We show the corresponding values of temperature in Fig. 9 as thick bars. Although it is difficult to draw any firm conclusion, the evolution of temperature does suggest that dust heating can contribute towards raising the gas temperature in Lyα absorbers as required by these observations. Note that an alternative explanation for increase of the minimal Doppler width with decreasing z has been suggested recently by Giallongo (1997) as a result of a decrease of the softness parameter in the framework of the photoionized heating model (Ferrara & Giallongo 1996).

A note on the uncertainties in our calculations arising from our assumptions concerning the background radiation is in order here. Unlike simple photoionization heating via dust grains is proportional to the intensity of the background radiation. This makes our calculations sensitive to the uncertainties in the background radiation, which include uncertainties in the QSO luminosity function, the contribution from young galaxies and the opacity of Lyα systems. As an example, using the LA model of absorption from Lyα clouds of Meiksin & Madau (1993) (see Sethi & Nath 1997), instead of model A3 of Giroux & Shapiro (1996), would increase the background flux and the dust heating rate.

Since dust heating rate is proportional to the flux of photons, we would expect a rise in temperature in absorbing systems close to quasars. The uncertainties in various parameters, however, may make this prediction difficult to test. Another prediction of our calculation is that, with a large scatter in the metallicity and

also in the value of $z_{\rm in}$, there would be a scatter in the temperature and in the minimum width in the distribution of b at a given redshift.

As we have shown in Section 3, if there is a low-density 'intercloud' part of the IGM, then the thermal evolution of this component of the IGM would be much different with the inclusion of dust heating than if only photoionization heating were used. This heating would also depend on the metallicity, and the metallicity of the IGM is not expected to be homogeneous. Nath & Trentham (1997) have estimated the probability distribution function of metallicity in the IGM, in the case of IGM enrichment from galactic winds, and found the standard deviation of the metallicity to be of the order of $0.01\,{\rm Z}_\odot$. Rauch et al. (1997) from the comparison of data with their numerical simulation found a scatter of an order of magnitude in the metallicity of Lyα absorbers. Therefore, it is reasonable to assume that there are regions in the IGM with higher dust content than we have considered above, and so hotter in general. (Of course, the actual temperature would depend on the thermal history of the region.)

Finally, we estimate the metallicity that is needed for dust heating to be more important than photoionization of a primordial gas. From Fig. 6, we estimate this lower limit for the accepted QSO type spectrum to be $Z/{\rm Z}_\odot \gtrsim 10^{-2.5}\,(n/10^{-5}\,{\rm cm}^{-3})\,(J_{912,-21}/0.5)^{-0.7}$, when the grain mixture is dominated by silicates (as in LMC or SMC type of mixture).

4.3 Feedback from IGM with dust heating

The feedback of the intergalactic medium on the process of galaxy formation is an interesting phenomenon and has been discussed by several authors. The reionization and reheating of the intergalactic medium inhibit the formation of small galaxies by the suppression of cooling and because of the high temperature of the IGM gas (Efstathiou 1992; Thoul & Weinberg 1996). Here we briefly discuss the implications of dust photoelectric heating for such feedback mechanisms.

First, unlike photoionization heating of a primordial gas, the dust photoelectric heating is proportional to the UV background radiation intensity. Fluctuations in the intensity and spectrum of the background radiation would result in variation in the inhibiting efficiency. However, even for silicates and for QSO type spectrum, the gas temperature is expected to change only by a factor of $\sim$1.5, thereby increasing the Jeans mass by a factor of $\sim$2. The dependence of the dust heating on the dust-to-gas ratio, however, has more interesting effects. When dust heating dominates in gravitationally confined (i.e. with constant or growing density) clouds, and the cooling is determined mainly by bremsstrahlung emission, $\Lambda(T) \propto T^{1/2}$, the gas temperature can be estimated from equation (28) as

$$T \propto \mathcal{D}^{(\alpha+\beta+1)/(\alpha+\beta)} J^{2/(\alpha+\beta)} n^{-2/(\alpha+\beta)}, \tag{32}$$

where $\mathcal{D}$ is the dust-to-gas ratio. Therefore, the enrichment of the gas (higher $\mathcal{D}$) results in the increase of gas temperature (and Jeans mass, $M_{\rm J} \propto \mathcal{D}^{3(\alpha+\beta+1)/2(\alpha+\beta)}$), and thus suppresses subsequent formation of low-mass galaxies. One can speculate from these simplified arguments that dust heating tends to suppress the progressive enrichment of the IGM with heavy elements. However, if the metallicity of enriched IGM gas exceeds a critical value $\zeta > \zeta_{\rm c}$, when radiative cooling from heavy elements dominates over bremsstrahlung cooling, metal-enriched regions cool efficiently and dust heating does not work any more as a negative feedback. For cooling as a result of C IV, which is the most dominant heavy element for cooling in these conditions, we estimate that $\zeta_{\rm c} \sim 0.05\,(n/10^{-4})^{-1}$, for $J_{912,-21} = 1$, $\alpha = 1$ and $T = 5 \times 10^4$ K. Note also that dust heating can work as a positive feedback (stimulating formation of regions of low temperature because of thermal instability) if hard spectrum ($\alpha \leq 0.5$) and large ($a \geq 0.01\mu$m) silicate grains dominate, though this case seems to be unrealistic.

5 CONCLUSION

We summarize our findings as follows:

(i) It is reasonable to associate dust grains with the metallicity observed in high-redshift Lyα absorbing systems, as the probability of the survival of dust grains during the process of spreading the metals and dust in the IGM and in the Lyα systems is high.

(ii) With the presence of the UV background radiation at high redshift, the dust particles in the IGM acquire charges that are much larger than is typical in the ISM, especially because of the low density of gas and high intensity of hard UV and X-ray photons. We illustrate this effect using two models of the UV background radiation, described in Table 1. Figs 1 and 2 show the dependences of the grain potential on gas density and grain size for graphites and silicates. Silicates in general have larger charges, and harder spectra help to produce larger grain potentials.

(ii) This results in a higher mean energy of the photo-ejected electrons, and therefore yields an important source of heating of the IGM gas. We show the volume heating rate as functions of the gas density, grain size distribution and grain type. Silicates fare better as heating agents, and smaller grains dominate the heating rate in general. We estimate that dust heating would be important for our QSO type spectra for a metallicity $Z/{\rm Z}_\odot \gtrsim 10^{-2.5}\,(n/10^{-5}\,{\rm cm}^{-3})\,J_{912,-21}^{-0.7}$.

(iv) Using these heating rates, and grain mixtures of the LMC type, we compute the temperature evolution of the gas in overdense regions of the IGM, with overdensity of $\sim$10, for various initial redshifts, initial temperatures and metallicities. We assume that the Lyα systems evolve in a passive manner, driven by the evolution of the background UV radiation and the boundary condition of the cloud expansion. We show the evolution for overdense regions that (a) adiabatically expand and keep the overdensity constant and (b) are confined either by shocks or gravity and keep the (proper) density constant. The difference in the temperatures in the cases when dust heating is included and when it is not, is of order of a factor of $\sim$2 for our hard QSO type spectra, for a metallicity of $Z/{\rm Z}_\odot = 0.01$ in a Hubble time at $z \sim 3$ for $\Omega_{\rm b} = 0.03$.

(v) We have speculated on the connection between the dust heating in such systems and the observed increase in the minimum width of Lyα absorption lines in time (most probably indicative of increase in the gas temperature). We have also discussed the possible increase in the gas temperature of Lyα absorption systems near QSOs as a result of increased UV flux, and the patchiness in the temperature of the IGM as a result of (a) density inhomogeneity and the (b) inhomogeneity in the metallicity.

ACKNOWLEDGMENTS

We thank A. Ferrara and E. E. Salpeter for valuable discussions and the anonymous referee for his comments. YS acknowledges the hospitality of IUCAA, India, where this work began, the hospitality of Astronomisches Institut, Ruhr Universität, Bochum, during the final stages of the work, and financial support from Italian Consiglio

Nazionale delle Ricerche within NATO Guest Fellowship programme 1996 (Ann. No. 219.29).

REFERENCES

Bajtlik S., Duncan R. C., Ostriker J. P., 1988, ApJ, 327, 520
Bakes E. L. O., Tielens A. G. G. M., 1994, ApJ, 427, 822 (BT)
Bechtold J., 1994, ApJS, 91, 1
Boyle B. J., 1991, Ann. N. Y. Acad. Sci., 647, 14
Carr B. J., Bond J. R., Arnett W. A., 1984, ApJ, 277, 445
Cen R., 1992, ApJS, 78, 341
Cen R., Simcoe R. A., 1997, ApJ, 483, 8
Ciardi B., Ferrara A., 1997, ApJ, 483, L5
Cooke A. J., Espey B., Carswell R. F., 1996, MNRAS, 284, 552
Cowie L. L., Songaila A., 1998, Nat, 394, 44
Cowie L. L., Songaila A., Kim T. S., Hu E. M., 1995, AJ, 109, 1522
Cristiani S., D'Odorico S., Fontana A., Giallongo E., Savaglio S., 1995, MNRAS, 273, 1016
Davidsen A. F., Kriss G. A., Zheng W., 1996, Nat, 380, 47
Draine B. T., 1978, ApJS, 36, 595
Draine B. T., 1989, in Bonetti A., Greenberg J. M., Aiello S., eds, Proc. Int. School of Physics 'E. Fermi', Evolution of Interstellar Dust and Related Topics. p. 91
Draine B. T., Lee H. M. 1984, ApJ, 285, 89
Draine B. T., Salpeter E. E., 1979, ApJ, 231, 438 (DS)
Dwek E., 1998, ApJ, 501, 643
Dwek E., Smith R. K., 1996, ApJ, 459, 686
Efstathiou G., 1992, MNRAS, 256, 43P
Fall S. M., Pei Y., 1989, ApJ, 337, 7
Fall S. M., Pei Y., McMahon R. G., 1989, ApJ, 341, L5
Ferrara A., Dettmar R.-J., 1994, ApJ, 427, 155
Ferrara A., Giallongo E., 1996, MNRAS, 282, 1165
Ferrara A., Nath B., Sethi S., Shchekinov Yu., 1998, MNRAS, in press
Field G. B., 1965, ApJ, 142, 531
Giallongo E., 1997, in 13th IAP, Structure and Evolution of the IGM from QSO Absorption Line Systems. In press
Giroux M. L., Shapiro P., 1996, ApJS, 102, 191
Gnedin N. Y., Ostriker J. P., 1997, ApJ, 486, 581
Haardt F., Madau P., 1996, ApJ, 461, 20
Haehnelt M. G., Rauch M., Steinmetz M., 1996, MNRAS, 283, 1055
Hogan C. J., Weymann R. J., 1987, MNRAS, 225, 1
Hogan C., Anderson S., Rugers M., 1997, AJ, 113, 1495
Jakobsen P., Boksenberg A., Deharveng J. M., Greenfield P., Jedzrejewski R., Paresce F., 1994, Nat, 370, 35
Jones A. P., Tielens A. G. G., Hollenbach D. J., 1996, ApJ, 469, 740
Kim T., Hu E. M., Cowie L. L., Songaila A., 1997, AJ, 114, 1
Kronberg P. P., 1994, Rep. Prog. Phys. 57, 325
Lisenfeld U., Ferrara A., 1998, ApJ, 496, 145
Loeb A., Haiman Z., 1997, ApJ, 490, l571
McKee C. F., 1989, in Alamandola L. J., Tielens A. G. G. M., eds, Proc. IAU Symp. 135, Interstellar Dust. Kluwer, Dordrecht, p. 431
McKee C. F., Hollenbach D. J., Seab C. G., Tielens A. G. G. M., 1987, ApJ, 318, 674
Madau P., 1992, ApJ, 389, L1
Mazzini A., di Serego Alighieri S., 1996, A&A, 311, 79
Meiksin A., Madau P., 1993, ApJ, 412, 34
Miralda-Escudé J., Ostriker J. P., 1990, ApJ, 350, 1
Miralda-Escudé J., Rees M. J., 1994, MNRAS, 266, 343
Miralda-Escudé J., Rees M. J., 1997, ApJ, 478, 57
Miralda-Escudé J., Cen R., Ostriker J. P., Rauch M., 1996, ApJ, 471, 582
Nath B., Trentham N., 1997, MNRAS, 291, 505
O'Donnel J. E., Mathis J. S., 1997, ApJ, 479, 806
Pei Y., 1992, ApJ, 395, 130
Pei Y., Fall S. M., Bechtold J., 1991, ApJ, 378, 6
Pettini M., King D. L., Smith L. J., Hunstead R. W., 1997, ApJ, 478, 536
Rauch M., Haehnelt M., Steinmetz M., 1997, ApJ, 481, 601
Reimers D., Kohler S., Wisotzki L., Groote D., Rodriguez-Pascual P., Wamsteker W., 1997, A&A, 327, 890
Rowan-Robinson M., Negroponte J., Silk J., 1979, Nat, 281, 635
Savaglio S., Cristiani S., D'Odorico S., Fontana A., Giallongo E., Molaro P., 1997, A&A, 318, 347
Schmidt K. H., Boller T., 1993, Astron. Nachr., 314, 361
Sethi S., Nath B. B., 1997, MNRAS, 289, 634
Shull M., Silk J., 1981, ApJ, 249, 26
Silk J., Wyse R. F. G., Shields G. A., 1987, ApJ, 322, L59
Songaila A., 1997, ApJ, 490, L1
Songaila A., 1998, AJ, 115, 2184
Songaila A., Cowie L. L., 1996, AJ, 112, 335
Songaila A., Hu E., Cowie L. L., 1995, Nat, 375, 124
Spitzer L., Jr, 1978, Physical Processes in the Interstellar Medium. Wiley, New York
Tegmark M., Silk J., Evrard A., 1993, ApJ, 417, 54
Thompson D., Djorgovski S., 1995, AJ, 110, 982
Thompson D., Mannucci F., Beckwith S. V. W., 1996, AJ, 112, 5
Thoul A., Weinberg D. H., 1996, ApJ, 465, 608
Tytler D., 1988, in Blades C., Turnshek D., Norman C., eds, QSO Absorption Lines: Probing the Universe. Cambridge Univ. Press, Cambridge, p. 179
Tytler D., Fan X.-M., Burles S., Cottrell L., Davis C., Kirkman D., Zuo L., 1995, in Meylan G., ed., QSO Absorption Lines. Springer-Verlag, Berlin, p. 289
Vainer B. V., 1990, SvA, 34(2), 107
Verstraete L., Léger A., d'Hendecourt L., Dutuit O., Deforneau D., 1990, A&A, 237, 436
Williger G., Baldwin J., Carswell R., Cooke A., Hazard C., Irwin M., McMahon R., Storrie-Lombardi L., 1994, ApJ, 428, 574
Zdziarski A., Johnson W. N., Done C., Smith D., McNaron-Brown K., 1995, ApJ, 438, L63
Zhang Y., Meiksin A., Anninos P., Norman M. L., 1998, ApJ, 495, 63
Zuo L., Beaver E. A., Burbidge E. M., Cohen R. D., Junkkarinen V. T., Lyons R. W., 1997, ApJ, 477, 568

This paper has been typeset from a TEX/LATEX file prepared by the author.